PUBLICATIONS OF THE ASTRONOMICAL SOCIETY OF THE PACIFIC
103: 1097–1108, October 1991

GAIN CALIBRATING NONUNIFORM IMAGE-ARRAY DATA USING ONLY THE IMAGE DATA

J. R. KUHN, H. LIN, AND D. LORANZ
Department of Physics and Astronomy, Michigan State University, East Lansing, Michigan 48824

Received 1990 July 23, revised 1991 July 30

ABSTRACT

An algorithm is developed for calibrating the spatial nonuniformity of image-array (CCD-type) detectors. Like other techniques this approach uses multiple, spatially displaced images. In circumstances where high-precision flat fields are not available by other means (i.e., sky flats) this technique is advantageous as it uses the data frames for gain calibration even when the array images extended, nonuniform, sources. Numerical experiments and direct observations with intrinsically uniform and quite nonuniform detectors show that this algorithm is useful when data frames are crowded with sources—circumstance where "median filtering" flatfielding techniques often fail. The algorithm described here is robust and efficiently uses information from multiple data frames to determine pixel gain variations, as we demonstrate using visible and IR array observations of extended sources.

Key words: data analysis–CCD flatfielding

1. Introduction

Mackay (1986) aptly states in his review of charge-coupled detectors (CCDs) that "the only uniform CCD is a dead CCD". Our experience is consistent with his observation and motivates the following discussion.

Astronomically useful imaging detectors can be quite linear (cf. Leach et al. 1980). It is not unusual for CCD detectors to show less than a 1% gain variation over a dynamic range of 10^3. Thus, in the following discussion we assume that individual picture elements (pixels) are linear but that pixel-to-pixel gain variation may be large. Indeed, experiments with an IR array, discussed below, were successful even when the pixel gain variations were of order unity. The algorithm we discuss is useful for computing the variation in the gain between pixels. Here we use the term "gain" to refer not only to the detector responsivity but also to optical or other image-plane variations that contribute to the spatial inhomogeneities in the optical sensitivity of pixel elements. We will also assume that the zero-point response, the signal produced by a null image (i.e., the output signal normally associated with dark current, amplifier bias, etc.), has been subtracted from the data. In practice array detectors are not strictly linear because of other "defects". Many of these "nonlinearities", like deferred charge effects, variable amplifier bias, charge-transfer problems, cosmic rays, saturation, etc., are addressed elsewhere (cf. Mackey 1986; Gilliland & Brown 1988; Howell 1989; Jacoby 1990). Our subject here is a technique for calibrating spatial pixel-to-pixel gain variations from array data. Tyson (1986) describes another useful discussion of this calibration problem. The technique described here complements his "median filter" approach. This technique seems to work well on calibration images of crowded stellar fields or observations of extended surface brightness sources.

The general approach to calibrating the pixel-to-pixel nonuniformity in the gain of live CCDs is called "flat-fielding" and often involves illuminating the array with a source which produces a spatially uniform light flux at the detector. Astronomers use several techniques to generate a uniformly bright image (cf. Mackay 1986) but, in general, the spatial calibration using these techniques will be only as accurate as the uniformity of the flat field. This is often a limiting systematic. A common astronomical technique uses flat fields obtained by observing out-of-focus screens (e.g., "dome" flats). We find that out-of-focus diffusers are practically limited to an accuracy of about 1%. It is difficult to do better because the optical configuration of the diffuser (and ray paths) is not identical to the actual data-taking configuration of the system. Telescopic observations of the twilight sky or longer integrations on blank night sky are better. In this case several blank images may be averaged or, better, median filtered to remove obvious illumination variations, such as stars. This is the approach Tyson (1986) used to calibrate small-scale gain variations at a level near 10^{-4}. If integration time is precious then there is some advantage to using the data frames to obtain the calibration, rather than spending significant time observing blank sky fields. The wavelength dependence of the optics and CCD response also requires that the uniform calibration field should have the same color as the data to be flatfielded. Our efforts in this paper to minimize some of these problems were motivated by astronomical CCD applications, although the following discussion may also be useful for solving the corresponding calibration problem in other multielement or areal detectors.

In many circumstances multiple, displaced images (perhaps the same as the signal frames) can be efficiently used to obtain the pixel gain to within a spatially constant factor. That this is true in principle follows from a simple observation. Assume that three images are obtained: an undisplaced image and two others obtained by shifting the CCD vertically and then horizontally by 1 pixel. The image is only displaced between pictures and we assume that we can subtract the zero-point response (the deferred charge, dark current, and amplifier bias level, etc.) from each pixel. Since each horizontal (vertical) pair of pixels is illuminated by the same flux between successive horizontally (vertically) displaced pictures, we know the ratio of the gain of every pair of contiguous pixels on the chip. Equivalently, we know the vertical and horizontal spatial derivatives in the logarithm of the gain function. Now, since we know the gradient of the log-gain function, we can integrate this to compute the logarithm of the gain to within an additive constant. Thus, we determine the gain to within an overall multiplicative factor.

In practice it may be difficult to displace an image by exactly one pixel, nor is this optimum for most applications. One might also question how systematic illumination variations between frames affect the solution and how multiple and arbitrarily displaced images should be used to minimize statistical and systematic noise in this gain computation. In the following sections we describe a more general least-squares algorithm that solves for the relative pixel gain function. We test this technique using an idealized detector and a Monte Carlo calculation in Section 3. In Section 4 we use the method with real optical array data, and in the last section we summarize the results.

2. Derivation of the Algorithm

We assume that an array can be treated as a collection of perfectly linear detectors—the gain of each element is independent of the input signal. In practice one can restrict the dynamic range of a data frame to yield a calibration which may vary with mean signal strength. Thus, if each pixel has a significant nonlinear response the practical application of this technique involves computing different gain tables as a function of mean illumination level. If several image fields are combined, as described below, this can be easily accomplished by only including pixels within a specified intensity range, if there is a large enough dynamic range in each observation. The practical application of this to nonlinear detectors is described below.

We also require that the null input response at each pixel can be measured and has been subtracted from the data so that the response of a pixel at $\mathbf{x}$ is

$$d_i(\mathbf{x}) = g(\mathbf{x}) s_i(\mathbf{x}) \ . \tag{1}$$

Here d_i, s_i, and g are the observed data, incident signal, and actual pixel gain at $\mathbf{x}$ on the array detector. The vector $\mathbf{x}$ identifies a pixel in a coordinate frame fixed to the detector, and the subscript i identifies a particular picture in a series $i = 1 \ldots N$. If the image is shifted by a vector $\mathbf{a}_i$ between exposures then we can also write $s_i(\mathbf{x}) = s(\mathbf{x} - \mathbf{a}_i)$, where $s(\mathbf{x})$ is some fiducial image. Thus, we assume that the image function does not change between observations. It follows from these definitions that $d_i(\mathbf{x} + \mathbf{a}_i)/d_j(\mathbf{x} + \mathbf{a}_j) = g(\mathbf{x} + \mathbf{a}_i)/g(\mathbf{x}+\mathbf{a}_j)$. Since the function g is independent of i, the observed d_i overdetermine the gain function. A least-squares solution for the gain is straightforward. Let upper-case symbols represent the logarithm of corresponding quantities defined above, then we seek a solution for $G(\mathbf{x})$ that minimizes

$$\sum_{i<j,\mathbf{x}} [D_i(\mathbf{x} + \mathbf{a}_i) - D_j(\mathbf{x} + \mathbf{a}_j) - G(\mathbf{x}+\mathbf{a}_i) + G(\mathbf{x} + \mathbf{a}_j)]^2 \ . \tag{2}$$

While this equation is correct for most of the pixels of a large detector array, the edges or terms involving displacements to nonexistent or insensitive pixels require a slight complication of equation (2). Similarly, if we are interested in computing the gain over a limited intensity range (because the detector may be nonlinear over a large range) then pixels with a signal strength that is too high or low are also treated in equation (2) as "missing" pixels. By using several images in equation (2) over a range of mean intensities a gain "function" could be computed for each pixel to make nonlinear corrections. This equation is exactly correct if the sum runs over terms for which the arguments of each of the bracketed functions correspond to valid, in-range, pixel coordinates. If either $\mathbf{x} + \mathbf{a}_i$ or $\mathbf{x} + \mathbf{a}_j$ is not a valid pixel then none of the terms for that particular i and j and $\mathbf{x}$ contribute. The derivative of equation (2) with respect to $G(\mathbf{x})$ gives

$$\begin{aligned} &\sum_{i<j} [G(\mathbf{x}) - G(\mathbf{x} - \mathbf{a}_i + \mathbf{a}_j) - D_i(\mathbf{x}) + D_j(\mathbf{x}-\mathbf{a}_i + \mathbf{a}_j)] \\ &+\sum_{i<j} [G(\mathbf{x}) - G(\mathbf{x} - \mathbf{a}_j + \mathbf{a}_i) + D_i(\mathbf{x} - \mathbf{a}_j + \mathbf{a}_i) - D_j(\mathbf{x})] = 0 \ . \end{aligned} \tag{3}$$

Here the first sum is over all distinct pairs i and j such that $\mathbf{x} - \mathbf{a}_i + \mathbf{a}_j$ is a valid pixel. The corresponding restriction that $\mathbf{x} - \mathbf{a}_j + \mathbf{a}_i$ be a valid pixel holds for the second bracketed term in equation (3).

An exact solution to equation (3) is difficult. We have constructed solutions by iterating from the solution $G^0(\mathbf{x}) = 0$. Thus, the solution at iteration $r + 1$ is given by

$$G^{r+1}(\mathbf{x}) = K(\mathbf{x}) + \frac{1}{n(\mathbf{x})}\sum_{i<j}\left[G^{r}(\mathbf{x}-\mathbf{a}_i+\mathbf{a}_j) + G^{r}(\mathbf{x}-\mathbf{a}_j+\mathbf{a}_i)\right] \quad (4)$$

with

$$K(\mathbf{x}) = \frac{1}{n(\mathbf{x})}\sum_{i<j}\left[D_i(\mathbf{x}) - D_j(\mathbf{x}-\mathbf{a}_i+\mathbf{a}_j)\right] + \left[D_j(\mathbf{x}) - D_i(\mathbf{x}-\mathbf{a}_j+\mathbf{a}_i)\right] .$$

Again, both terms in each bracket must have valid arguments for either term in the bracket to contribute to the sum. The function $n(\mathbf{x})$ is the total number of bracketed terms in equation (3) that contribute to the total sum. For pixels that are not linked to invalid pixels by the displacements we have that $n(\mathbf{x}) = N(N-1)/2$.

Equation (4) has the form of a relaxation solution to Poisson's equation. The iterated solution at a given pixel is derived from the average of surrounding pixels from the previous iteration. Indeed, for the limiting problem of determining the gain from three images displaced 1 pixel in orthogonal directions it can be shown that the solution solves a 2-dimensional Poisson equation. It is also worth noting that in this case the solution is invariant under a gauge transformation of the form $G'(\mathbf{x}) = G(\mathbf{x}) + \phi(\mathbf{x})$, if $\phi(\mathbf{x})$ satisfies the Laplace equation $\nabla^2\phi(\mathbf{x}) = 0$.

For arbitrary $\mathbf{a}_i$ equation (4) is not a Poisson equation but there is a corresponding (more restrictive) gauge freedom in the gain solution. With arbitrary $\mathbf{a}_i$, when $G(\mathbf{x})$ is a solution of equation (4), then

$$G'(\mathbf{x}) = G(\mathbf{x}) + \vec{\beta}\cdot\mathbf{x} \quad (5)$$

is also a solution for an infinite pixel domain with no gaps. Thus, to the extent that the relaxation solution does not propagate information from the boundaries of the array into the center, the gain solution may not be unique. In practice this means that the solution must be iterated for as many times as it takes to shift the smallest displacement across the full range of the array. The pure square symmetry is also broken by "missing" pixels which will also tend to reduce the number of iterations required to minimize the gradient ambiguity.

The precise constraints on the pixel domain and displacement vectors $\mathbf{a}_i$ which lead to a unique solution for $G(\mathbf{x})$ are not easily determined. Nevertheless, as long as the gain solution converges to a level consistent with our statistical noise estimates, any ambiguity in $G(\mathbf{x})$ is an honest consequence of missing information in the original data. So how does one, a priori, choose displaced data frames so that no gain information is lost? Part of the answer is obvious, e.g., the vectors $\mathbf{a}_i$ should not be colinear. It is also clear that if the displacements between frames are multiples of a common factor then adjacent pixels are not "linked" by the iteration algorithm. Thus, displacements should (ideally) have no common multiples. Beyond this we have pursued an empirical "solution" to the problem of demonstrating the utility of the technique.

The largest systematic error we have encountered with real data appears when successive image frames do not have the same mean signal level because of, for example, exposure time variations. Flat fields obtained by averaging or median filtering of the data frames are also somewhat sensitive to this systematic, but it is not hard to see that with the relaxation solution it is possible for temporal changes to be modulated into false spatial gain variations. As we argue below, this systematic may appear as a gradient in the logarithm of the gain. If there are large mean signal level variations between frames then each data frame must be scaled to have the same mean signal level before solving for the gain.

If the mean intensity level were allowed to vary, then, instead of equation (1), we obtain

$$d_i(\mathbf{x}) = g(\mathbf{x})s_i(\mathbf{x})\alpha_i' \ , \quad (6)$$

where α_i' are multiplicative constants which parameterize the variations in the mean intensity level of each frame. In this case we replace $G(\mathbf{x})$ with $G'(\mathbf{x})$ of equation (5), then equation (2) becomes

$$\sum_{i<j,\mathbf{x}}\left[D_i(\mathbf{x}+\mathbf{a}_i) - D_j(\mathbf{x}+\mathbf{a}_j) - G(\mathbf{x}+\mathbf{a}_i) + G(\mathbf{x}+\mathbf{a}_j) - \vec{\beta}\cdot(\mathbf{a}_i-\mathbf{a}_j) - \alpha_i + \alpha_j\right]^2 , \quad (7)$$

where α_i are the log of the α_i'. The last three terms $C = \vec{\beta}\cdot(\mathbf{a}_i - \mathbf{a}_j) - \alpha_i + \alpha_j$ in equation (7) are a constant for any pair of frames, i, j. Thus the α in equation (7) may be minimized by a nonzero β which minimizes the equation for C. In fact if $C = 0$ for all i and j and some β then our solution for the gain differs from the solution for the gain when the systematics were negligible ($\alpha_i = 0$) only by a linear gradient.

3. Results from Simulated Data

We have checked the numerical properties of equation (4) by generating artificial data arrays that simulate ideal linear response detectors. We used these data to learn how the solution depends on (1) spatial structure in the calibration image and similar structure in the detector response, (2) the signal-to-noise ratio in each pixel measurement, (3) the number of pixels, (4) the number of image displacements and their magnitude, and (5) the number of iterations used to obtain a solution. By using simulated data we can directly compare the derived gain (from eq. (4)) with the exact array response that was used to generate the data. One measure of the relative success of the algorithm is the standard deviation

$$\sigma = \sqrt{\Sigma(G^r(x) - G_{\rm true}(x))^2/N}$$

where $G_{\rm true}(x)$ is the logarithm of the actual gain and N is the number of pixels.

Displaced images were obtained by integral shifts of the simulated CCD gain function. All of the calculations described here used a discrete domain so that subpixel interpolation was not necessary. In real applications (see below) images cannot be obtained with displacements of exact integral numbers of pixels. The routines we have implemented do not interpolate to subpixel resolution so that real data must be oversampled or short-range structure in the images must be ignored or removed before the gain can be calculated.

Figure 1 shows how the gain approaches the actual solution as a function of iteration and noise level. In these plots shot noise has been simulated by adding a random value to each pixel measurement. In each case the "noise" was uniformly distributed with amplitude as indicated. These calculations used nine images displaced by ± 3 and ± 5 pixels in the horizontal and vertical direction. The simulated CCD had a 10% pixel-pixel gain (QE) variation. The simulated image was either a central Gaussian or a random (uniformly distributed) nearly flat image. Several points should be noted. Perhaps the most important is that the curves in this figure are negligibly affected by adding significant spatial structure to the flat image. For example, when a Gaussian spike (maximum of 30 times the background, half-width of three pixels) or a flat image with only 1% spatial noise are simulated, the solutions for the gain yield the same standard deviation at any given iteration, to within 10^{-4}. The convergence rate, which is approximately a power law in iteration count, r, decreases more slowly beyond a critical number of iterations, r_c, and σ seems to approach a limiting value. Small r_c values can be obtained for all the cases shown in Figure 1 except for the two with photon noise less than 0.5%. In these two examples the convergence is still decreasing at approximately its initial rate after 100 iterations. For the other cases r_c is less than 15 iterations.

As expected, the limiting gain error σ_{limit} and the convergence rate are functions of the number of displacement frames. In general, both σ_{limit} and the convergence rate improve as the number of frames increases, and, of course, σ_{limit} improves with the per-pixel signal-to-noise ratio of the individual frames, while the convergence rate

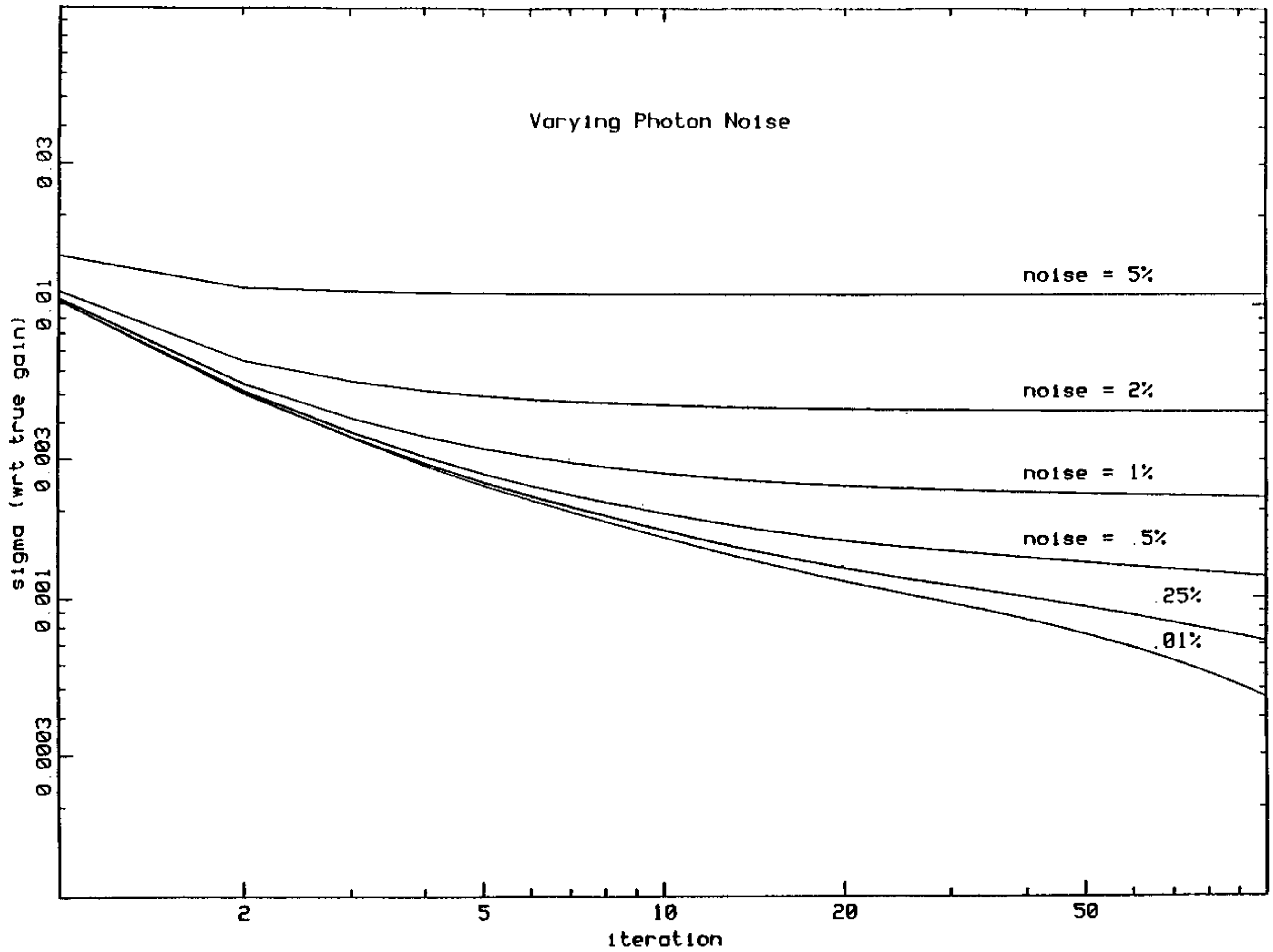

FIG. 1–For all cases in this figure: (1) the simulated image had 1% photon, (2) the simulated detector had 10% spatial gain noise, (3) the camera was 100 by 100 pixels, and (4) there were nine displaced images of ± 3 and ± 5 pixels horizontally and vertically.

improves as the data arrays get smaller. Both quantities are only weakly dependent on the displacement magnitudes. We have run many simulations using a range of array size, displacement magnitude, signal-to-noise ratio, and number of frames. In all cases with a (per-pixel) noise of at least 0.25% the limiting gain noise in the algorithm is within a factor of 1.5 of the theoretical minimum flat-field gain noise. The number of iterations required to attain this accuracy decreases with increasing number of frames, but for nine displaced frames ten iterations were almost always adequate. For astronomical CCD observations using arrays near 500×500 pixels in size and with 1% shot noise, nine observations displaced by a few pixels yield a calibration whose "noise" is within a factor of two of the theoretical noise limit. It is also clear that the range of parameters which yields good, if not optimal, performance is conveniently broad. It is generally possible to obtain the gain with rms errors that are within a factor of 2 or 3 of what is ultimately possible.

4. Results from Real Data

Actual imaging detectors do not have the ideal characteristics described in the previous section, or may have other pathological problems which could render this algorithm useless in practice. In fact, detectors show a wide range of "pathologies" and we have not done an exhaustive test of this technique with a large number of devices. On the other hand we have had good luck using this iterative technique to flat field several detector/camera/telescope optical systems. We routinely calibrate optical and near-infrared images which use a TI4849 390×584 CCD, an SAIC/FORD 1024×1024 CCD, and a Rockwell TCM 1000C 128×128 HgCdTl infrared array. The following section describes how we have applied results from Sections 2 and 3 above to some real data.

We now calibrate our array data using these techniques whenever possible. Although we have found systematic problems with data that may require attention before the gain can be computed using equation (4), in general, the final product using these techniques (a "flat field") has been as good or better than we could obtain by other means (including sky flats, "median" flats, or "dome" flats).

In general the practical application of the iteration technique closely follows the analysis described above: data frames are corrected for the zero-point response (dark and bias frame subtraction), natural logarithms are computed, and equation (4) is iterated. The only practical change we have made in implementing the algorithm is to dynamically specify an allowable signal intensity range for all pixels. Thus, if the signal of any pixel is outside this range, that pixel is ignored in that term of the solution. Thus, the detector response can be easily measured as a function of mean intensity. This is important for calibrating nonlinear detectors and has been useful as a simple filter for the input data. The relative shift between images was determined from the peak in their cross correlation. The image displacements were rounded to the nearest pixel.

The practical limitation to the technique comes from systematic variations between data frames. The principal systematics we have encountered seem to be: seeing variations (which change star profiles), sky-level variations (which may change the sky background level), or small shutter-speed changes (which may affect the overall exposure level of the image). In general these systematics may be a concern when calibrating to better than 1%.

High-contrast objects in an image (like stars) are sensitive to atmospheric seeing variations and in many astronomical observations are spatially undersampled in the image. Thus, as our analysis does not interpolate to subpixel scales (nor make any assumption on the effective stellar profiles), it is important that star profiles be smoothed or removed before calculating the gain. We have computed flat fields from defocused images, but this approach then no longer has the advantage inherent to computing the gain from useful data frames. The solution we have adopted is to ignore all pixels above some intensity threshold (as in more conventional calibrating techniques). The threshold is chosen from, for example, a histogram of the pixel intensity values to discard the high-intensity tail (4σ) of the distribution. As we show below, faint small-scale features do not corrupt the iterated gain calculation.

A second noticeable systematics occurs when the light level changes between images. This may appear as a spatial gradient in the solution and can be fit for and removed a posteriori. A better solution is to correct the data frames to the same mean intensity before iterating. We do this by correcting the mean of the log of the data to the same value in the corresponding overlap region of each frame. A systematic least-squares technique for making this correction is described in Boughn & Kuhn (1986). We find that this correction is important if the mean signal variations divided by the square root of the number of data frames are larger than the desired accuracy of the calibration.

The CCD camera uses a Photometrics, Inc., cryogenic dewar and camera readout electronics. The Ford CCD has pixel-pixel quantum efficiency variations of a few percent and a couple of defective columns. The read noise is about eleven electrons which corresponds to about one ADU. The stellar data described below were obtained in a 750–850 nm wavelength band using the Michigan State University (MSU) 0.6-m $f/8$ Boller and Chivens telescope at the Michigan State University Observatory. The dewar was mounted at the Cassegrain focus of the Ritchey-Chrétien telescope, 4 cm behind the filter.

Figure 2 shows one of nine 5-minute exposures of M 53. The images were displaced randomly, ranging by an amount between 4 and 206 pixels in the vertical and horizontal directions. The mean sky level was about 350 ADU and varies from image to image by as much as 20%. Each image was normalized by an additive offset to yield a constant mean sky level between frames. Data values larger than 400 ADU were ignored to remove bright stars in the gain computation.

A running value of σ was computed from the difference of $G(x)$ between successive iterations. We found that σ dropped approximately like a power law in the iteration count with an exponent of -0.8. By the sixth iteration σ decreased two orders of magnitude, while between the sixth and fiftieth iterations, it only decreased a factor of seven.

The resulting log of the gain after ten iterations is shown in Figure 3. Here the range from dark to light corresponds to the range between -0.05 and 0.025 in the log of the gain. For comparison a median flat field was also computed using the same data. The difference between logarithms of the iterated and median flats is displayed in Figure 4. The range from dark to bright in this figure is -0.0014 to 0.0014.

Figure 3 shows small "gain" variations resulting from both detector variations and optical imperfections (like the dust ring visible in the lower-left corner). Figure 4 shows that the median flat field does differ from this solution. The standard deviation of the difference is 0.0036. We also can see "ghosts" of faint stars in the difference image which have leaked through the median filter. The difference between the median flat and an out-of focus screen (or "dome") flat confirms that the residual "ghost" structure we see in the median flat field is absent in the iterated flat. The iterated gain is insensitive to these faint stars, while, in this case, the median flat field would introduce errors at the 0.4% level.

Observations of continuous surface brightness objects (like resolved image of the Sun) are especially suited for calibration with this technique. We obtained images of the Sun to compare the iterated flat-field calibration with one obtained by observing the sky. These data were obtained with the camera system described above, but with a TI 4849 390 $\times$ 584 CCD at wavelengths of 650 $\pm$ 5 nm. A low-scattered-light telescope and fast shutter were used to obtain observations of the Sun and sky using

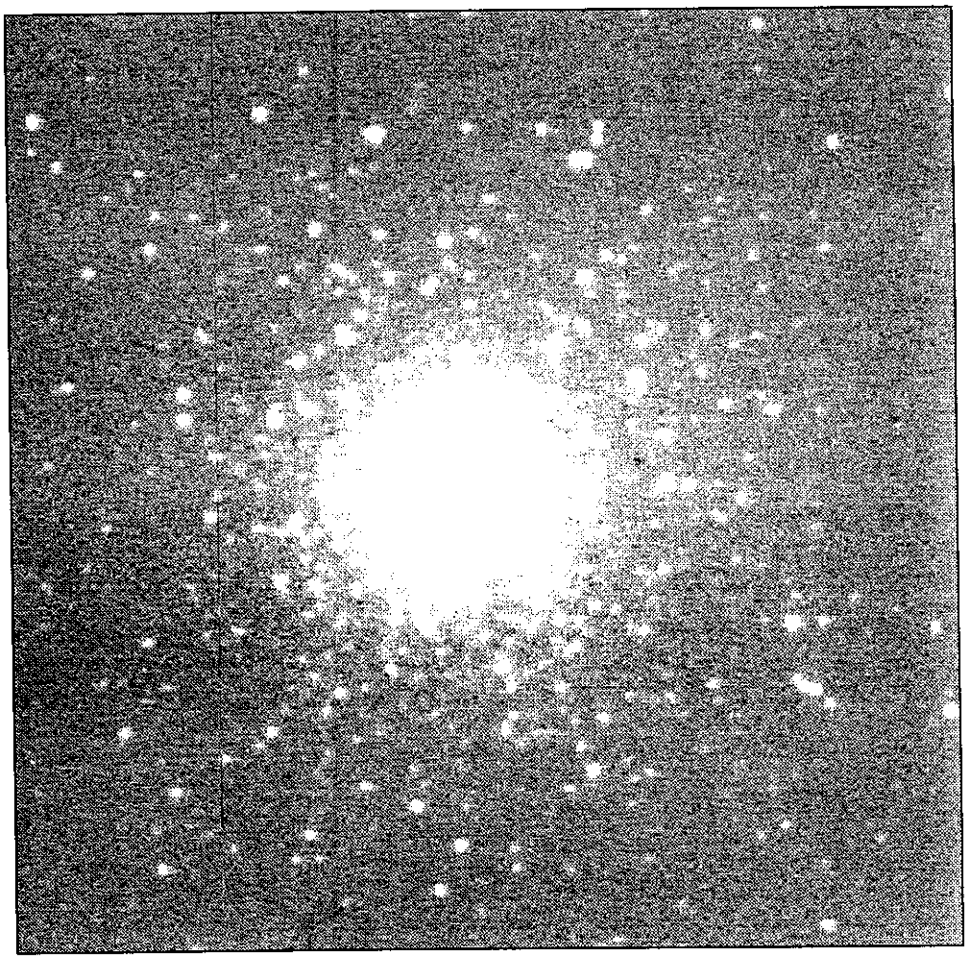

FIG. 2–An uncorrected M 53 image. This is a 5-minute exposure obtained with the Ford array and the MSU 0.6-m telescope. Several dust rings are visible at the lower part of the image.

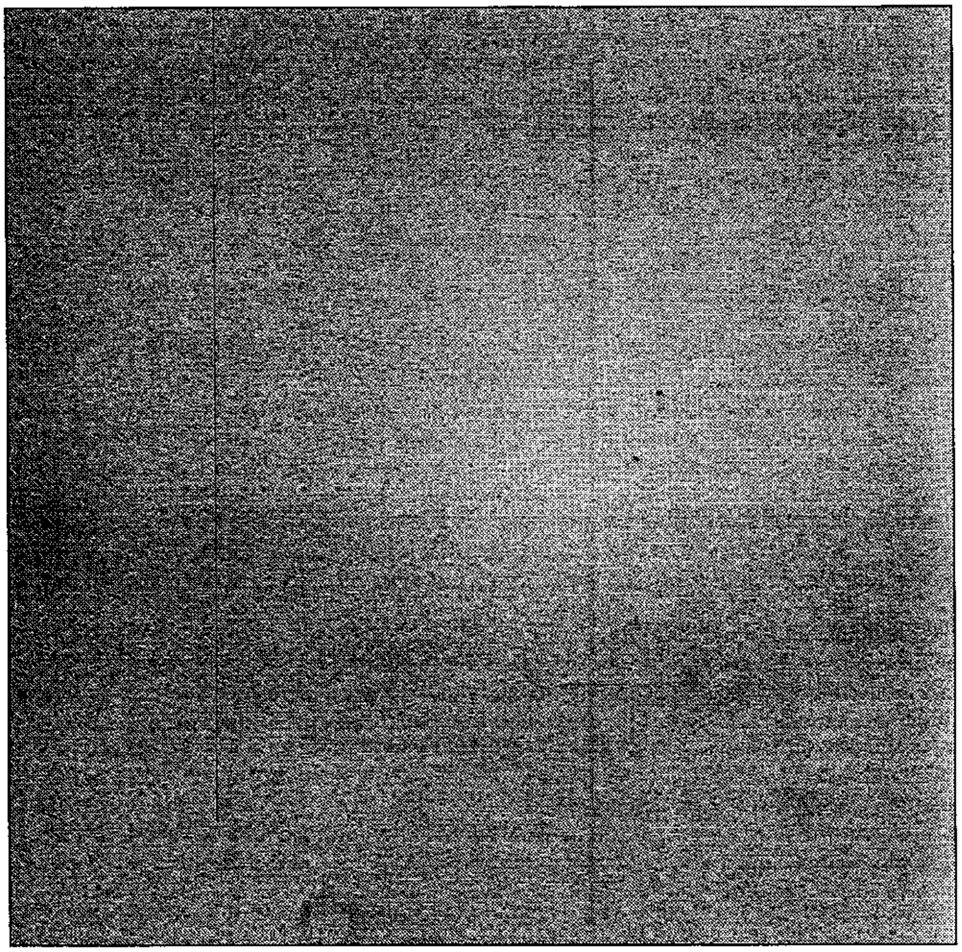

FIG. 3–The log of the iterated gain after the tenth iteration. The gray-scale range is −0.05 to 0.025 from dark to bright. Nine displaced images like Figure 2 were used to compute this flat field.

identical optics and filters. Figure 5 shows an image of the Sun taken with this system. A series of nine displaced images were obtained with random horizontal and vertical displacements ranging between 26 and 360 pixels. Pixels near the sharp limb of the Sun were discarded by ignoring data with signal levels below a threshold determined by the solar limb-darkening function. In these data the mean level of each image changed by a few percent, due to the changing transparency of the sky. The logarithm of each image was normalized by an additive constant which was also determined by least squares (Boughn & Kuhn 1986). Figure 6 shows the log of the gain solution after ten iterations. As before we see optical imperfections ("dust" rings), column segments, and random pixel-pixel quantum efficiency variations of a few percent. The dark spots are regions without coverage, either because it is outside the solar limb or it is the discarded sunspot area. There is still some residual structure (gain error) aligned with the limb due to the errors in the transparency adjustment. Comparing the iterated gain solution with a sky flat shows that there is some structure in the gain error with an amplitude of about 4×10^{-3}. The standard deviation of the difference in the log of the iterated and sky flats is 0.002. This is within a factor of 2 of the theoretical noise limit.

Both CCDs described above show relatively small efficiency variations of a few percent. We also use this technique to calibrate an IR array (which uses a switched FET readout) that has comparatively large QE variations of between 25% and 90%. The infrared system is a Rockwell TCM 1000C 128 × 128 infrared array operating at liquid-nitrogen temperature, with an H-band (1.6 microns) broad-band (0.5 micron FWHM) filter mounted inside the dewar. Figure 7 shows a raw solar image (dark subtracted) in the H band. The infrared array has a very large gain variation as manifested by the fingerlike pattern extending from the upper-right corner to the center of the field, as well as the systematic bright and dark pattern from column to column. Using the sky as the flat field for the infrared observations is practically impossible in view of the very long integration time required to obtain a single sky flat since the sky brightness during the day

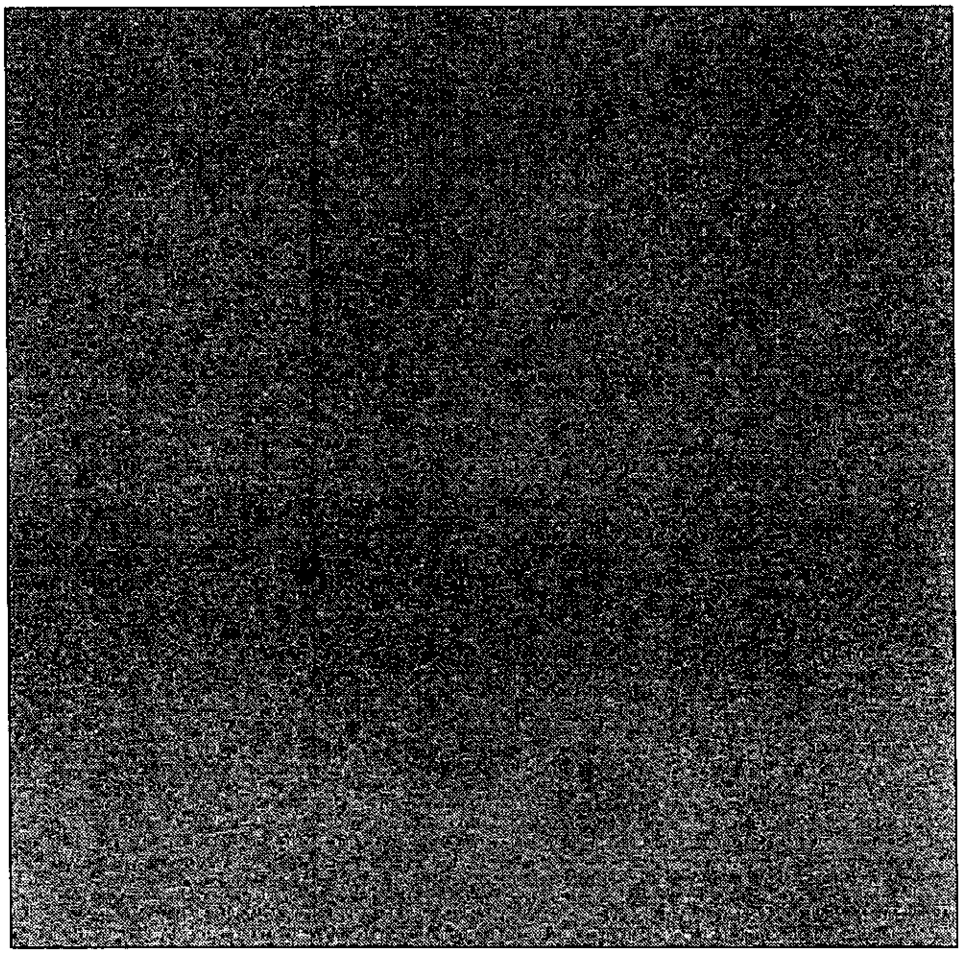

FIG. 4–The difference between the iterated gain of Figure 3 and a median gain that was calculated using the same nine displaced data frames. The display range is ± 0.0014. The magnitude of this error is approximately 4×10^{-3} and is due to faint stars in M 53 which bias the median flat but do not affect the iterated flat field.

is considerably fainter than the solar brightness in the infrared.

We calculated the gain field of the infrared array to the tenth iteration with a set of ten displaced solar images. To avoid the sharp limb only data within the inner 0.8 solar radius were used for the calculation. The sunspots were also discarded by applying a lower intensity threshold. The iterated gain field is shown in Figure 8. Close inspection of the flat field shows some residual structure (gain error) aligned with the limb with a magnitude of approximately 1×10^{-3}. This is within our error budget and is much smaller than the systematic flat-field errors we obtained using diffuser flats.

5. Conclusion

We have demonstrated a new technique for calibrating image-array data. It may be useful for observations requiring especially good flat-field calibration of images of extended surface brightness targets. The technique efficiently uses the available information from the array data to construct the best least-squares gain estimate.

We are grateful to Horace Smith for obtaining the test frames of M 53. This work was supported by NASA through contract NAS5-30386 and by the NSF through grant ATM 89-01689.

REFERENCES

Boughn, S., & Kuhn, J. R. 1986, ApJ, 309, 33
Gilliland, R. L., & Brown, T. H. 1988, PASP, 100, 754
Howell, S. B. 1989, PASP, 101, 616
Jacoby, G. H., ed. 1990, CCDs in Astronomy, PASPC, Vol. 8 (Chelsea, MI, Astr. Soc. of Pacific)
Leach, R. W., Schild, R. E., Gursky, H., Madejski, G. M., Schwartz, D. A., & Weekes, T. C. 1980, PASP, 92, 233
Mackay, C. D. 1986, ARA&A, 24, 225
Tyson, J. A. 1986, J. Opt. Soc. Am. A, 3, 2131

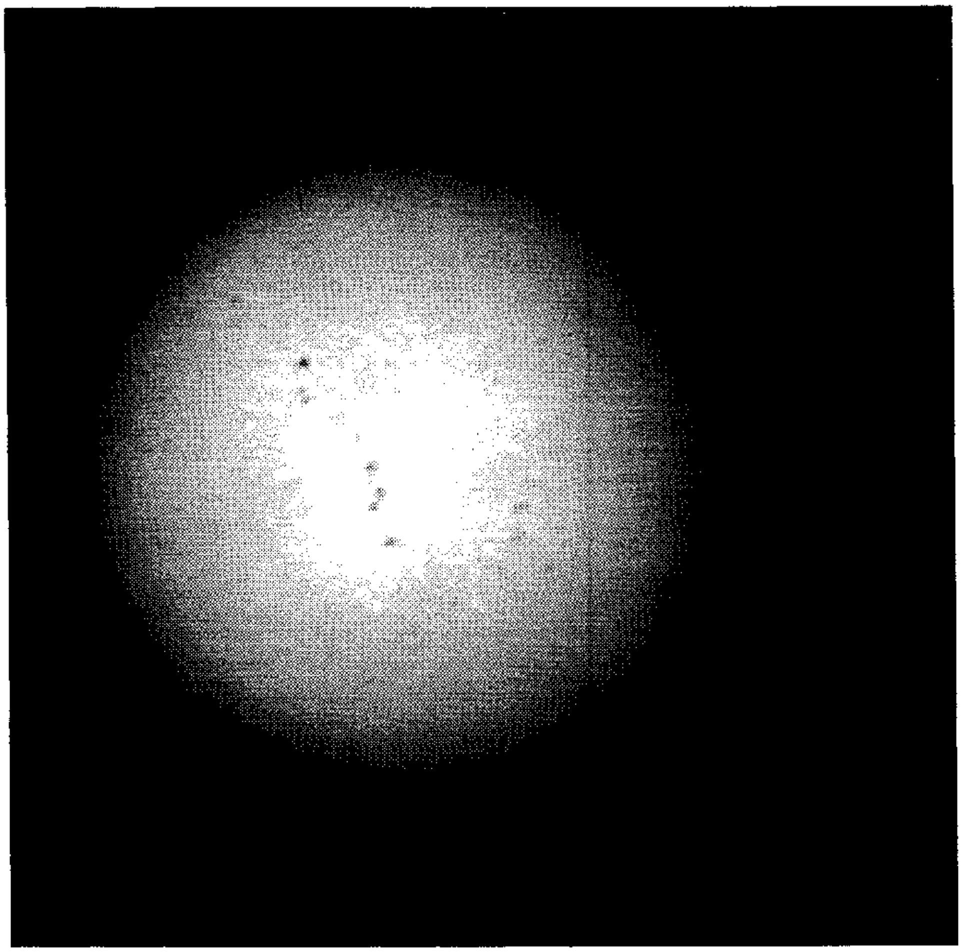

FIG. 5–An uncorrected solar image taken with a low scattered-light telescope. These data were obtained with a TI4849 CCD and a small refracting solar telescope. It shows sunspots as well as the gain pattern due to the optics and CCD.

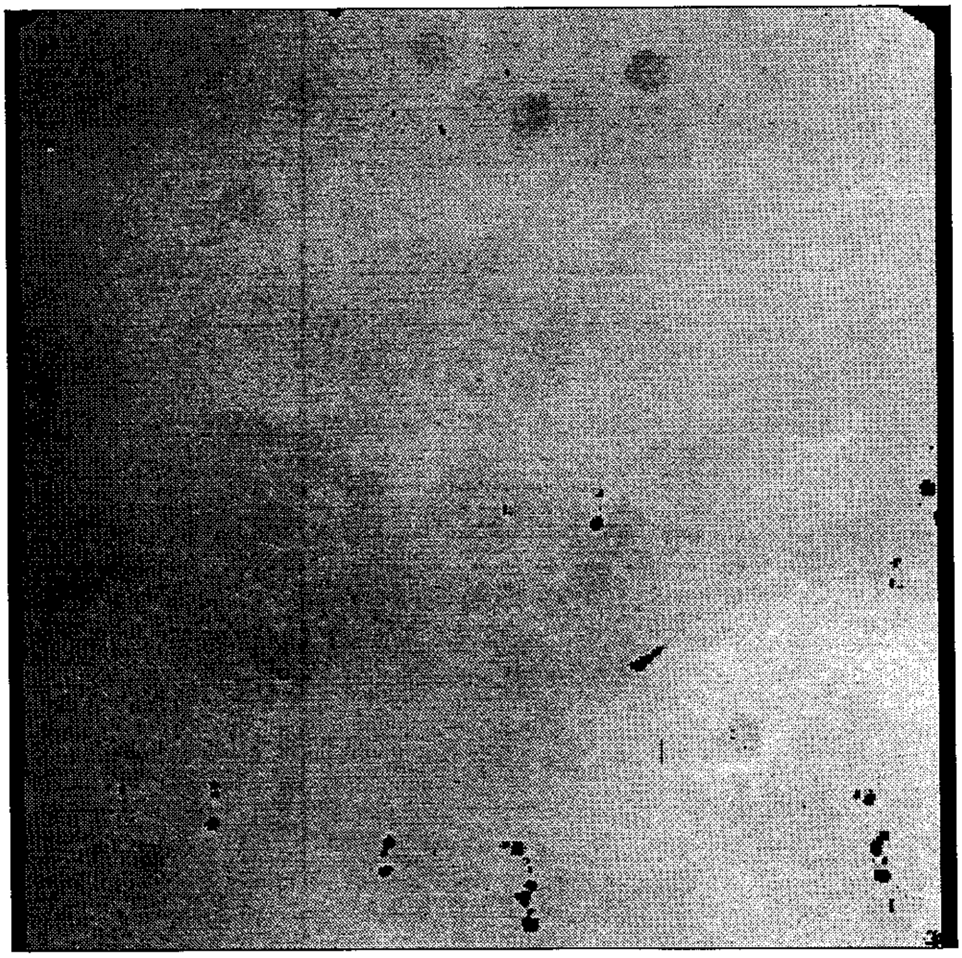

FIG. 6–The log of the iterated gain after the tenth iteration using nine displaced solar images. The gray-scale display range is from −0.1 to 0.05.

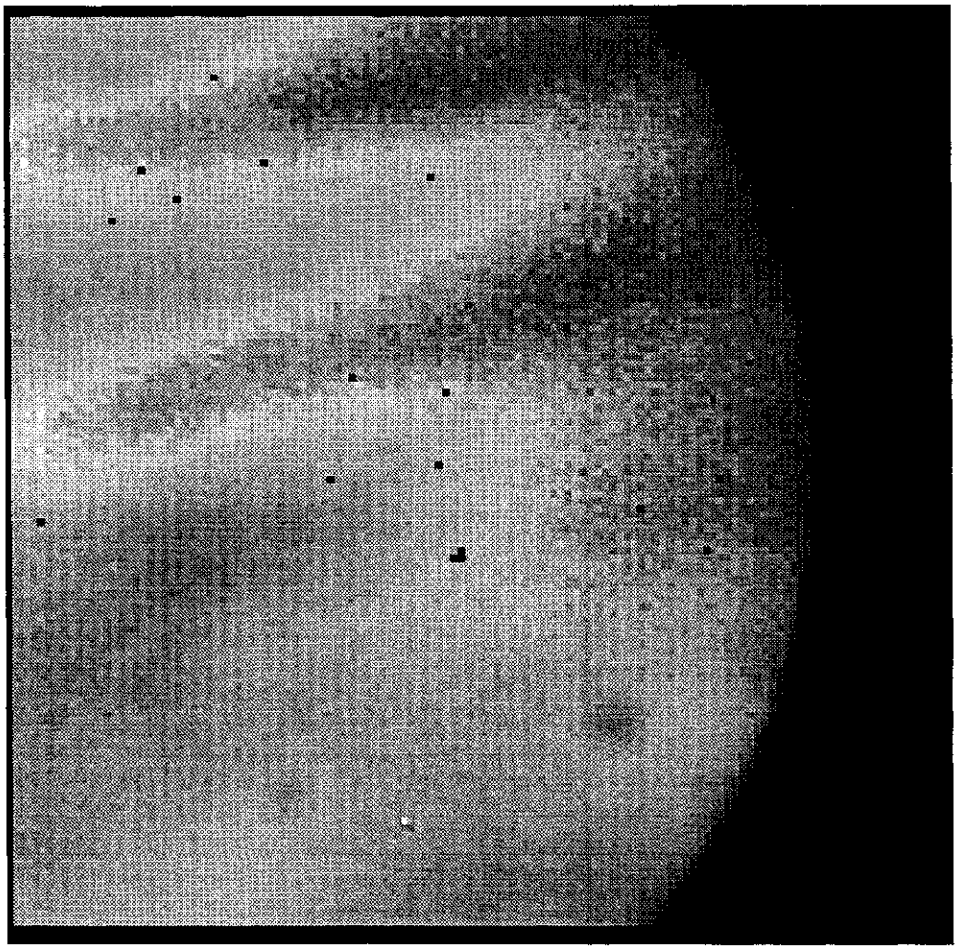

FIG. 7–An infrared solar image taken with the Rockwell array. The fingerlike pattern is due to large quantum efficiency variations across the array.

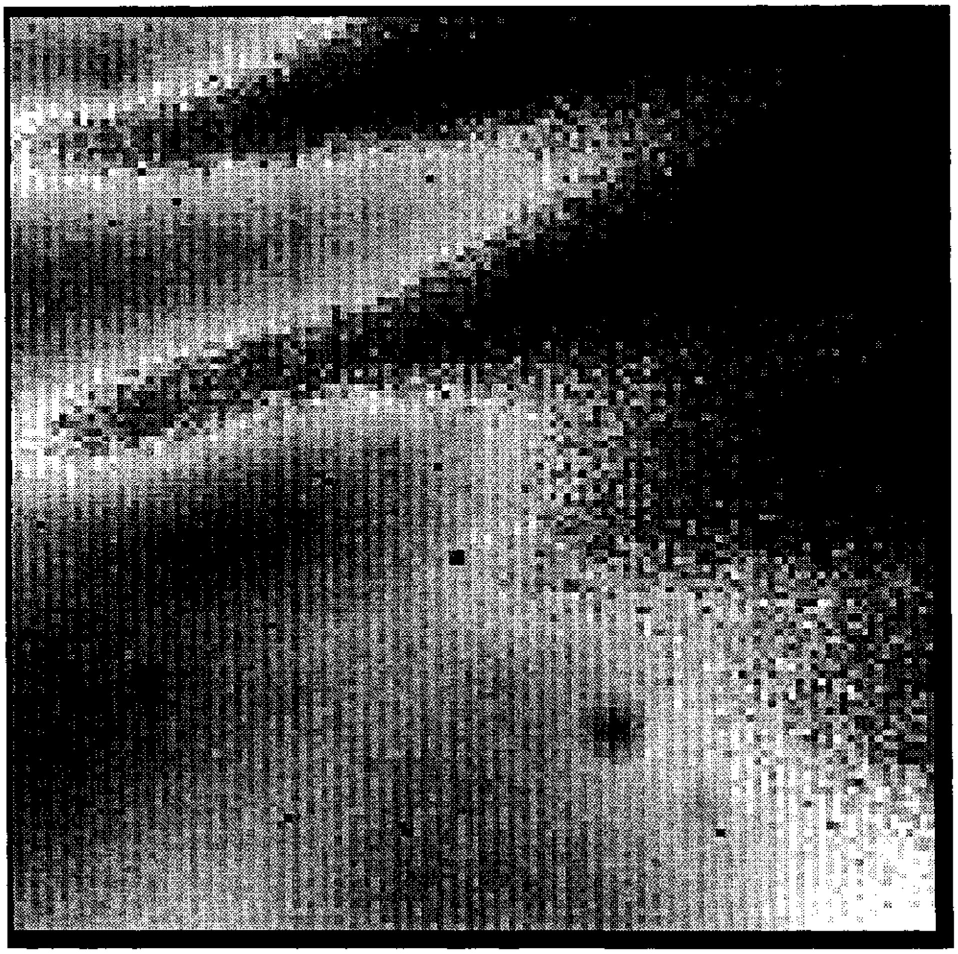

FIG. 8–The log of the iterated gain after the tenth iteration using ten IR solar images. The display range is from −0.5 to 0.5.